CRYSTAL GROWTH & DESIGN

Article

pubs.acs.org/crystal

Nucleation under Soft Confinement: Role of Polymer–Solute Interactions

Ying Diao, Matthew E. Helgeson, Zeina A. Siam, Patrick S. Doyle, Allan S. Myerson, T. Alan Hatton, and Bernhardt L. Trout*

Novartis-MIT Center for Continuous Manufacturing and Department of Chemical Engineering, Massachusetts Institute of Technology, 77 Massachusetts Avenue, E19-502b, Cambridge Massachusetts 02139, United States

Supporting Information

ABSTRACT: Nucleation of a crystalline phase almost always occurs at interfaces. However, the lack of fundamental understanding of the impact of interfacial properties on nucleation hinders the design of nucleation active materials for regulating crystallization in practice. In particular, the role of intermolecular interactions is often neglected in nucleation under confinement such as those provided by nano- and microporous materials. Herein, we report the use of a novel material, polymer microgels with tunable microstructure and chemistry, for understanding the role of intermolecular interactions in nucleation under confinement and for controlling crystallization from solution in general. We demonstrate that by tuning the polymer–solute interactions, solute nucleation kinetics were promoted by up to 4 orders of magnitude. Moreover, the effect of polymer–solute interactions was manifested by the split of nucleation time scales due to the presence of nucleation sites of distinct chemical compositions in the microgels, characterized by small angle neutron scattering. Our mechanistic investigations suggest that the polymer matrix facilitates nucleation by enhancing effective solute–solute interactions due to solute adsorptive partitioning and by promoting molecular alignment inferred from preferred crystal orientations on polymer surfaces. Our results provide new insights into nucleation at interfaces and help enable a rational material design approach for directing nucleation of molecular crystals from solution.

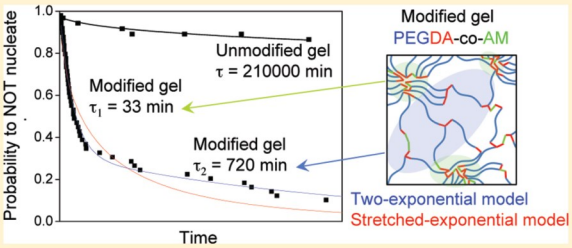

INTRODUCTION

Interfaces present in a metastable liquid are believed to have a profound impact on its nucleation behavior.[1] Considerable strides have been made over the last few decades toward understanding the effect of interfaces on nucleation, and several mechanisms have been proposed. The epitaxy mechanism has been well established to describe crystal formation on crystalline surfaces[2,3] or surfaces with two-dimensional symmetry.[4−6] Surfaces may also affect nucleation via polarization matching with the crystallizing molecule when both the surface and the crystal exhibit a net dipole across the surface/crystal interface.[7,8] This mechanistic understanding from these studies should provide guidance for designing surfaces to control crystal nucleation. However, the applicability of these approaches is restricted to a large extent because the surface properties involved are not freely adjustable for the systems of interest, such as 3D or 2D crystalline structures characteristic of crystal facets, self-assembled monolayers, and Langmuir–Blodgett films, etc. Noncrystalline polymeric materials offer a promising alternative, since their structure, topology, and chemistry are easily tunable over a wide range by a variety of established fabrication methods, as shown in our previous work.[9−11] In particular, we have demonstrated polymer gels with tunable microstructures to be exceptional materials for controlling nucleation kinetics.[9] The microgels exhibit a meshlike structure. With mesh sizes ranging from a few angstroms to several nanometers, the polymer network partitions the absorbed solution and restricts the mobility of adsorbed solute molecules, as such providing a confined environment for crystallization to take place. In contrast to rigid nanoporous materials previously reported for studying nucleation under confinement,[12−14] soft polymer gels are unique in their ability to concentrate solute molecules via thermodynamic partitioning driven by favorable polymer–solute interactions. Such interactions may hold the key to the effectiveness of polymer gels in promoting nucleation.

Intermolecular interactions were shown to play an important role in dictating nucleation behavior at interfaces.[10,15] For molecular crystallization on smooth substrates, previous studies reported selective nucleation of polymorphs by tuning the polarity or hydrophobicity of surface functional groups,[16,17] but even qualitative correlations have not been demonstrated unambiguously, let alone quantitative descriptions. In addition, the effect of intermolecular interactions is often neglected in studies on nucleation in confined environments such as those provided by nano- and microporous materials.[13,18,19] Overall, mechanistic understanding is still insufficient to enable rational

Received: October 29, 2011
Published: November 14, 2011

design of surface chemistry for controlling nucleation of molecular crystals from solution. The complexity arises partially from the weak intermolecular interactions in molecular systems relative to those in ionic, metallic, and covalent crystals, flexible molecular conformations, and intricate solvent effects. At complex interfaces, the influence of intermolecular interactions on nucleation is often convoluted with other factors such as surface lattice structures, surface morphology, etc., making it more challenging to study.

This work aims to elucidate the role of intermolecular interactions in nucleation at polymer−solution interfaces and their interplay with the effects of polymer microstructure on nucleation. To this end, we tuned the chemistry of polymer microgels via copolymerization and quantified its effect on nucleation systematically. We found that the nucleation kinetics of model compounds are very sensitive to the polymer−solute interactions, and a dramatic acceleration of nucleation was observed when the strength of the polymer−solute interactions was increased. Moreover, the functionalized microgels imparted a distinct signature to the nucleation induction time distributions, which featured two characteristic time scales, suggesting a possible chemical heterogeneity at the nanometer scale due to copolymerization. We further explored the underlying mechanism from the perspective of adsorptive partitioning and a templating effect to assist in the interpretation of the role of intermolecular interactions in gel-induced nucleation. We anticipate that our results will help advance the fundamental understanding of nucleation at complex interfaces in molecular systems and facilitate the rational design of materials for controlling nucleation from solution.

RESULTS AND DISCUSSION

Synthesis and Characterization of the Polymer Microgels. Two model polymer chemistries were chosen for the synthesis of microgel particles to use in our gel-induced nucleation studies. The first were cross-linked homopolymer gels of poly(ethylene glycol) diacrylate (PEG_MDA) of various PEG molecular weights, M (g/mol), ranging from 130 to 700 g/mol. The second were copolymers of PEGDA and 4-acryloylmorpholine (AM). AM was selected as a comonomer to functionalize the PEGDA gel because it contains multiple hydrogen bond acceptors, which may interact favorably with the hydrogen-bond donors of aspirin (ASA) and acetaminophen (ACM), the model compounds employed in this study. The synthesis of model microgel PEGDA and PEGDA-co-AM microgels was carried out using stop flow lithography (SFL) (see the Experimental Section and Supporting Information).[20]

The microstructure of PEGDA and PEGDA-co-AM gels was characterized via equilibrium swelling experiments and small angle neutron scattering (SANS). Figure 1 compares the average mesh sizes (ξ) from swelling measurements (closed symbols) measured previously for PEGDA microgels (blue)[9] to those obtained for PEGDA-co-AM microgels (red) with increasing M. We find that the incorporation of AM into the PEGDA network results in a mild increase in mesh size on the order of 10−25% over the range of PEG molecular weights studied. This is expected, since the effective lengthening of the acrylic polymer backbone by insertion of AM monomers is small as compared to the overall length of the PEG chains. The measured values of ξ (open symbols, Figure 1) from the SANS measurements (Supporting Information), performed on representative samples with M = 200 and 700 g/mol, are

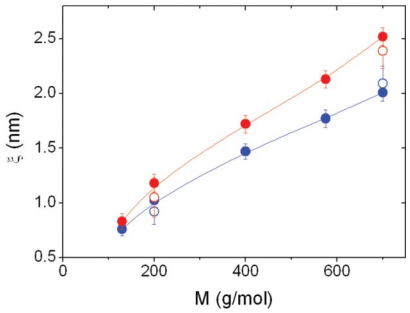

Figure 1. Average mesh size ξ of PEGDA (blue) and PEGDA-co-AM (red) microgels measured in 38/62 (v/v) ethanol/water at 23 °C estimated by equilibrium swelling measurements (closed symbols) and SANS analysis (open symbols).

generally in fairly good quantitative agreement with those measured by equilibrium swelling measurements.

Quantification of Polymer−Solute Interactions. The strength of intermolecular interactions between the PEGDA-co-AM polymer network and solute was characterized in terms of the solute equilibrium partition coefficient under the same conditions as used in the crystallization study. The solute partition coefficient κ, defined as the ratio of the solute mass fraction in the solution confined in the gel to that in the bulk, is a relevant parameter because it informs the solute concentration in the gel under crystallization conditions, which is an important factor affecting nucleation. Shown in Figure 2a, κ for

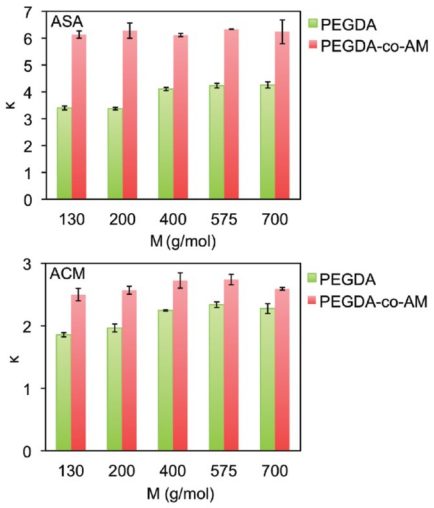

Figure 2. Comparison of partition coefficient, κ, in the PEGDA gels vs PEGDA-co-AM gels for ASA (top) and ACM (bottom) systems. κ is defined as the ratio of solute mass fraction in the solution confined in the gel to that in the bulk. The error bars are calculated from three to four independent repeats.

ASA increased by 60% on average after introducing AM into the PEGDA gel, and the ASA concentration in the PEGDA-co-AM gels reached as high as six times that of the bulk solution. This result indicates much stronger interactions between the ASA and the polymer matrix after functionalization. It is also worth noting that before chemical modification, κ climbed from 3.4 to around 4.2 with the increase in M, the PEG molecular

weight of the PEGDA monomer, while after modification, κ became insensitive to M. This observation suggests that ASA interacts mainly with the AM segments of PEGDA-co-AM polymers in the solution environment, as discussed below. The PEGDA polymers are comprised of the PEG subchain and the polymerized acrylate cross-linkers. As M increases, the mass ratio of PEG to acrylate increases, and so does κ in the case of the PEGDA system, indicating that ASA primarily associates with the PEG subchain. This inference is further supported by the fact that the molar ratio of ethylene oxide units in PEG to ASA, calculated from the partition experiments, remained constant (7.7) for all mesh sizes. In the case of PEGDA-co-AM, the mass fraction of AM did not change with M_n, and correspondingly, κ was also invariant, yielding a constant AM-to-ASA molar ratio of around unity. This result provides strong evidence that ASA interacts preferentially with AM rather than with PEG or the acrylate groups constituting the polymer gel.

The ASA–polymer interactions were further quantified with the solute adsorption enthalpy via isothermal titration calorimetry (ITC), which also helps to deepen the understanding of partitioning effect. Figure 3 shows the results of ITC measurements, where the enthalpy of interaction between ASA and both $PEG_{400}DA$ and $PEG_{400}DA$-co-AM microgels is plotted versus the equilibrium concentration of ASA. The data are presented both as instantaneous enthalpies at a given concentration, $\Delta H_{ASA-gel}$ (top), and as cumulative enthalpies up to a certain concentration, $\Delta H^{tot}_{ASA-gel}$ (bottom). At low ASA concentrations, $\Delta H_{ASA-gel}$ exhibits a plateau for both PEGDA and PEGDA-co-AM gels. After titration of ASA to a concentration of 10 mM or greater, $\Delta H_{ASA-gel}$ decreases monotonically, approaching zero at large ASA concentrations. This behavior suggests that the mechanism of ASA–polymer interactions is by adsorption of ASA onto the polymer network. This is particularly apparent when examining the cumulative interaction enthalpy, $\Delta H^{tot}_{ASA-gel}$, which exhibits the qualitative features of an adsorption isotherm, such that $\Delta H^{tot}_{ASA-gel}$ is related to the equilibrium surface coverage of ASA on the polymer hydrogel. At low concentrations, the increase of $\Delta H^{tot}_{ASA-gel}$ with ASA concentration is roughly linear, corresponding to ideal adsorption of ASA where a majority of the injected solute molecules adsorb to the surface. However, at sufficiently large ASA concentrations, $\Delta H^{tot}_{ASA-gel}$ tends toward a plateau value, suggesting saturation of the hydrogel surface due to monolayer coverage of ASA. Attempts to fit simple, one-site adsorption isotherms to the data in Figure 3 were unsuccessful, most likely due to the complicated structure and chemistry of the hydrogel surface. Nevertheless, the considerable range of concentration over which $\Delta H^{tot}_{ASA-gel}$ increases linearly with the ASA concentration allows for the calculation of the enthalpy of adsorption of ASA at infinite dilution, $\Delta H^{\infty}_{ASA-gel}$, by averaging $\Delta H_{ASA-gel}$ over ASA concentrations in the plateau region (Figure 3), resulting in $\Delta H^{\infty}_{ASA-gel} = -9.8$ kcal/mol for $PEG_{400}DA$ and $\Delta H^{\infty}_{ASA-gel} = -12.3$ kcal/mol for $PEG_{400}DA$-co-AM. This confirms that ASA–polymer interactions are significantly more favorable for PEGDA-co-AM hydrogels as compared to PEGDA hydrogels and further suggests that the presence of the AM comonomer significantly enhances the adsorption of ASA.

The ACM–polymer interactions were much weaker than those in the ASA system for both of the microgels (Figure 2b), as indicated by the lower κ values. A marginal increase in κ was seen with the modified gels, ranging from 35 (M = 130 g/mol) to 14% (M = 700 g/mol). As with ASA, ACM partitioned to a similar extent to the modified gel for all mesh sizes, whereas in the unmodified gels, κ varied more strongly with M. This result may also imply that ACM interacts more strongly with AM than with PEGDA. On comparing the ASA to ACM systems, it is not obvious why the interactions of ASA with both the polymers were stronger than those of ACM. Inspecting their functional groups, one would expect the reverse since ACM has more hydrogen-bond donors, and both PEGDA and AM are rich in hydrogen-bond acceptors. Complementary functional group interactions, commonly used for interpreting substrate effects on nucleation from solution, fail to explain our observations, because they do not account for the fact that both the polymer and the solute are well solvated. The increased cost for desolvation of ACM relative to that of ASA required for adsorption onto the polymer may be the reason for the lower partitioning of ACM, since solute–solvent interactions are stronger for ACM than for ASA, as indicated by the higher ACM solubility in 38/62 (v/v) ethanol/water mixture (90 mg/mL at 25 °C) than that of ASA (32 mg/mL at 25 °C).

Effect of Polymer Gels on Nucleation Induction Time Statistics. The addition of polymer microgels in supersaturated solutions of ASA or ACM yielded crystals grown on the microgels, as observed under the optical microscope. We infer that nucleation occurs from inside the microgel, given significantly higher solute concentration inside the gel. However, only the nuclei formed near the gel surface can continue to grow out of the gel into a macroscopic crystal. This is because the diffusivity of solute confined in the gel is 2–3 orders of magnitude lower than that in the bulk solution, as we previously estimated.[9] Examination of crystals grown from the microgel using SEM revealed an intimate connection between the crystal and the gel interfaces (Figure S3 in the Supporting Information), suggesting that nucleation may have occurred from inside the gel, as we inferred. In all cases, the stable polymorph of ASA or ACM was obtained, with and without the presence of microgels, as confirmed by XRD using crystals harvested immediately after nucleation was detected.

To quantitatively evaluate the impact of polymer–solute interactions on nucleation kinetics, induction times of ASA and ACM were determined in the presence of microgels of different average mesh sizes and with and without chemical modification, suspended in supersaturated solutions of ASA or ACM. The volume fraction of microgels in the solution was so small ($\sim 10^{-5}$) that the solute partitioning in the gels did not affect the bulk concentrations. For each system, a large number of experiments (50–100) were conducted to obtain the induction time probability distribution. Ideally, the nucleation induction time should follow the Poisson distribution, verified in our previous work.[10] However, deviations can occur, as observed in this study, when there is more than one type of nucleation site in a sample, giving rise to multiple Poisson processes with different characteristic time scales.

For samples with PEGDA microgels, the nucleation induction time distributions can be faithfully described by stretched exponentials (Figure 4 and Tables 1 and 2), $P = \exp[-(t/\tau)^{\beta}]$, where P is the probability to observe no crystallization event within time t and τ is the average induction time. The stretched exponential exponent β serves as a measure of the spread of time scales[21] characterizing the nucleation process or the distribution of kinetic barriers[22] arising from heterogenieties in the system. In our system, such heterogenieties can be attributed to spatial variations in both the mesh size and the chemical composition of the microgel at

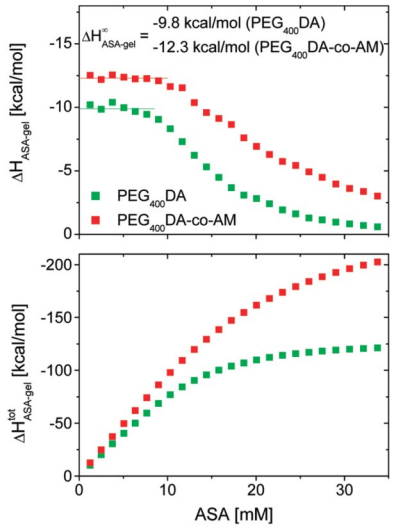

Figure 3. Enthalpy isotherms for adsorption of ASA onto $PEG_{400}DA$ (green) and $PEG_{400}DA$-co-AM (red) microgels, including instantaneous (top) and cumulative (bottom) enthalpies of adsorption. Straight lines give fits used to obtain the infinite dilution enthalpy of adsorption.

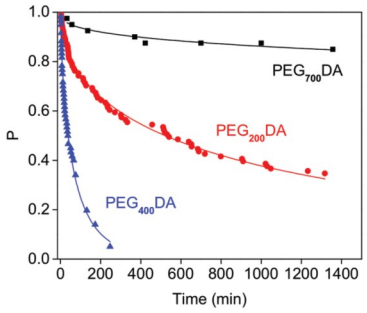

Figure 4. Nucleation induction time statistics for ASA in the presence of PEGDA microgels. P is the probability for no nucleation event to occur within time t. Experimental data are fitted with the stretched exponential model (solid lines). Representative examples are shown here, and the complete set of fitted parameters is listed in Table 1.

nanometer length scales. In all cases, we obtained β values significantly lower than unity, suggesting apparent deviations from the Poisson distribution $[P = \exp(-t/\tau)]$. As such, microgel-induced nucleation serves as an example of first-order phase transformation in the presence of quenched disorder, a phenomenon frequently observed but rarely investigated quantatitively. A common case of this phenomenon is heterogeneous nucleation on random impurities. In statistical physics terms, the PEGDA microgel displays quenched disorder in the sense that its mesh size and conformation distribute randomly, and such disorder is "quenched" meaning these features do not evolve with time.

It is interesting to note that β varies significantly with the average mesh size of the microgel. Previously, we found that the polymer mesh size has a profound impact on the nucleation kinetics, and there exists an optimum average mesh size corresponding to the fastest nucleation rate.[9] The largest value of β found was obtained at the optimum average mesh size for both ASA and ACM (Table 1, M = 400 g/mol; Table 2, M = 200 g/mol). This is probably because in microgels of the optimum average mesh size, the nucleation sites with the ideal mesh size and conformation where the majority of nucleation events take place become dominant in number and activity, leading to a narrower distribution of nucleation time scales; β should approach unity when the activity of a single type of nucleation site is so high that other nucleation sites are inactive by comparison.

Modification of PEGDA microgels with AM resulted in much faster ASA nucleation kinetics than in the absence of AM overall. The nucleation induction time distributions were better described by two-exponential models (Table 1 and Figure 5) than by the stretched exponentials obtained with PEGDA microgels. The two exponential processes yielded two distinct time scales, τ_1 and τ_2, with τ_1 an order of magnitude smaller than τ_2. Both of these processes were much faster than those obtained with PEGDA microgels, supporting our hypothesis that strong polymer−solute interactions lead to the overall success of polymer gels in promoting nucleation.

The creation of two time scales possibly results from the presence of two dominant types of active nucleation sites in PEGDA-co-AM microgels. The SANS analysis suggests that such nucleation sites of distinct nucleation activities may arise from significant structural heterogeneity over length scales ranging from 10 to 60 nm (Figure S1 and Table S1 in the Supporting Information). Although the nature of this heterogeneity is presently unclear, such structure typically arises from microphase separation within the gel.[23] In this study, we infer that the microphase separation may be driven by

Table 1. Comparison of Average Nucleation Induction Times for ASA in the Presence of PEGDA vs PEGDA-co-AM Microgels[a]

		M (g/mol)					
polymer	fitted parameters	bulk	130	200	400	575	700
PEGDA	τ (min)	not detectable	not detectable	1052	66.7	3500	210000
	β	NA	NA	0.52	0.69	0.52	0.36
	R^2	NA	NA	0.99	0.96	0.96	0.92
PEGDA-co-AM	τ_1 (min)	not detectable	170	21	39	51	33
	τ_2 (min)		4900	99	400	470	720
	a	NA	0.52	0.05	0.62	0.79	0.68
	R^2	NA	0.98	0.99	0.99	0.99	0.99

[a]Supersaturation S = 2.1. Induction time distribution data obtained with PEGDA microgels were fitted with stretched exponentials via nonlinear least square regression: $P = \exp[-(t/\tau)^{\beta}]$, where P is the probability to observe no crystallization event within time t. The R^2 value corresponding to $PEG_{700}DA$ samples is lower since much fewer samples crystallized within the experimental time frame. Induction time distribution data obtained with PEGDA-co-AM microgels were fitted with two exponentials via nonlinear least square regression: $P = a\exp(-t/\tau_1) + (1 - a)\exp(-t/\tau_2)$.

Table 2. Comparison of Average Nucleation Induction Times for ACM in the Presence of PEGDA vs PEGDA-co-AM Microgels[a]

		M (g/mol)				
polymer	fitted parameters	bulk	130	200	400	700
PEGDA	τ (min)	37000	1600	480	5300	37000
	β	0.50	0.54	0.72	0.50	0.50
	R^2	0.97	0.96	0.96	0.97	0.97
PEGDA-co-AM	τ_1 (min)	same as above	55	88	70	NA
	τ_2 (min)		1360	12400	35000	NA
	a		0.23	0.36	0.29	NA
	R^2		0.91	0.96	0.97	NA

[a]Supersaturation $S = 3.7$. Induction time distribution data obtained with PEGDA microgels were fitted with stretched exponentials via nonlinear least square regression: $P = \exp[-(t/\tau)^{\beta}]$. Induction time distribution data obtained with PEGDA-co-AM were fitted with two exponentials via nonlinear least square regression: $P = a\exp(-t/\tau_1) + (1 - a)\exp(-t/\tau_2)$.

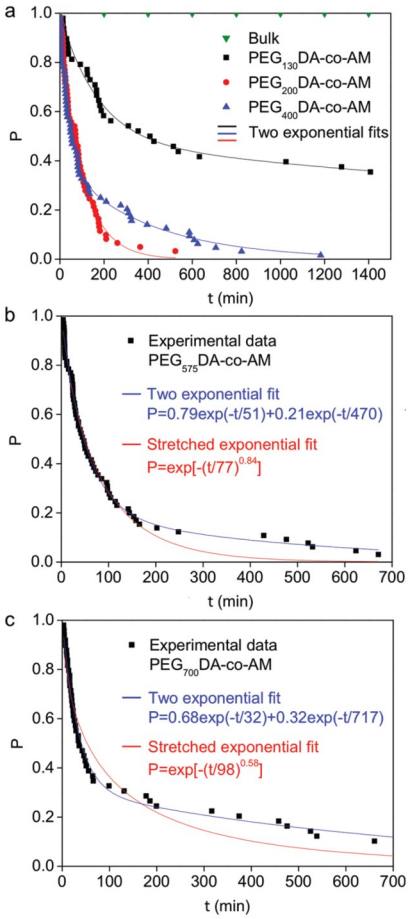

Figure 5. Effect of PEGDA-co-AM microgels on nucleation induction time statistics for ASA. P is the probability for no nucleation event to occur within time t. (a) Effect of polymer mesh size on nucleation kinetics. Fitted parameters for the two-exponential model are listed in Table 1. Data for M = 575 and 700 g/mol are shown separately for clarity. (b and c) Comparison of two-exponential vs stretched exponential models using PEG_{575}DA-co-AM (b) and PEG_{700}DA-co-AM (c) as representative examples.

the aggregation of the polymerized acrylate groups (Figure 6 and the Supporting Information). Because the addition of AM comonomer (green) within the gel must occur along the

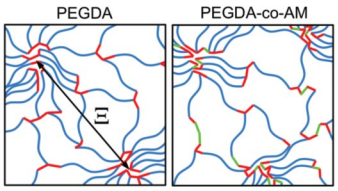

Figure 6. Schematics of microgel structures inferred from SANS measurements. Blue, red, and green chains denote the PEG subchain, acrylate, and AM segments, respectively.

acrylate backbone chains, the spatial distribution of AM groups will be strongly correlated with that of the acrylate chains. Thus, we expect that phase separation of the acrylate chains results in segregation of AM groups to the acrylate-rich regions.

On the basis of the inferred polymer microstructure (Figure 6), it is likely that the segregation of AM functional monomers into regions of high local acrylate density results in two largely different types of active sites for nucleation. One type, in the acrylate-lean (and thus AM-lean) regions of the gel, will be such that interactions between the solute and the PEG subchain will dominate the nucleation process. The other, in the acrylate and AM-rich regions of the gel, will be such that interactions between the solute and the AM will dominate the nucleation process. The latter AM-rich domains may serve as the more active nucleation sites due to favorable solute−AM interactions (as characterized by higher partition coefficients and adsorption enthalpies), which correspond to the shorter average induction times for ASA, and vice versa for the AM-lean domains. This interpretation is also consistent with the observation that the shorter time scale τ_1 is much less sensitive to the variation in the PEG molecular weight M than is τ_2, the longer time scale (Table 1), since the AM-rich domain should be less affected by variations in the PEG subchain length than would be the AM-lean domain. In the case of PEGDA microgels, although there also exists structural heterogeneity due to microphase separation between the acrylate-rich and the acrylate-lean domains, such a dramatic split of nucleation times scales was not observed, probably because only the acrylate-lean domains are nucleation active given that ASA interacts mainly with the PEG subchain in PEGDA, as discussed earlier. In other words, insertion of AM into the nucleation-inactive acrylate-rich domains turned the original state of quenched disorder into a more "ordered" state, characterized by two distinct types of nucleation active domains, in contrast to the original "random" distribution of nucleation sites. In PEGDA-co-AM microgels,

the quenched disorder in the PEG-rich domains should still be present; however, its effect on the nucleation induction time becomes insignificant when the AM-rich domains exhibit much higher nucleation activity.

Similarly, nucleation of ACM in the presence of PEGDA-co-AM microgels exhibited two exponential processes (Table 2), probably for the same reasons as discussed above. In contrast to the observations for the ASA systems, the slower time scale τ_2, possibly associated with the PEG rich, AM-lean nucleation sites, was no smaller than that obtained with the PEGDA microgels, although the faster time scale τ_1 was shortened by at least an order of magnitude as in the case of ASA. This observation indicates that the modification of PEGDA with AM promoted nucleation of ACM overall but to a lesser extent than with the ASA system. The data also suggest that the AM-rich nucleation sites are much more active than are the AM-lean ones, as evidenced by the 2 orders of magnitude difference between τ_1 and τ_2. However, such differences are not reflected in the partitioning results, where no significant improvement in the partition coefficients was seen following chemical modification. Other factors such as the templating effect may play a more important role in this case, as discussed later.

Several effects may have contributed to the observed enhancement in nucleation kinetics with chemically modified polymer gels. First, preferential partitioning increases solute concentration in the gel. Considering the adsorptive partitioning mechanism discussed earlier, a significant fraction of solute molecules are likely to be enriched around the polymer matrix via adsorption as opposed to being well solvated inside the gel. In addition, the solute may further concentrate in certain domains of the gel due to its chemical heterogeneity. Both factors lead to an increase in local solute concentration, which is expected to enhance effective solute−solute interactions. Although the higher solute concentration in the gel does not necessarily result in a larger supersaturation (as the chemical potential of the solute in the bulk and the gel must necessarily be equal at equilibrium), the polymer may enhance nucleation by lowering its kinetic barrier. In other words, the polymer may play the role of a nucleation "catalyst" via enriching solute at the polymer−solution interface to facilitate molecular cluster formation. Nucleation acceleration due to the "surface enrichment effect" has been reported in previous computational studies.[24,25] For instance, Van Meel[24] has shown via Monte Carlo simulations that at a disordered flat wall, the adsorption of a thin layer of globular particles facilitated their nucleation near the wall, because of a reduced free-energy barrier to nucleation.

The concentration effect discussed above suggests the observation that PEGDA-co-AM gels were much more effective than PEGDA in promoting ASA nucleation can be credited partially to higher average solute concentrations in the gel (Figure 2a), especially considering that the concentration in local domains may be even higher due to the chemical heterogeneity of the gel. In the ACM system, the average solute concentration increased only marginally in the modified gel (Figure 2b), and as such, its contribution to overall nucleation enhancement is less significant than in the case of ASA. However, it is still remarkable that by incorporating AM into the PEGDA matrix, a fast nucleation process was created with average induction times orders of magnitude shorter than those obtained with PEGDA alone (Table 2). It is difficult to attribute this phenomenon solely to the concentration effect, since even though the chemical heterogeneity polarizes the solute concentration between the AM-rich and the AM-lean segments, the extent of concentration polarization should be small, based on the fact that the partitioning coefficient did not increase much after replacing 50 v % of PEGDA with AM. Other contributing factors may include the difference in specific polymer−solute interactions (templating effect) or the nanoscale structural heterogeneity of the polymer gel. Below, we investigate the templating effect by analyzing the preferred crystal orientation on PEGDA and PEGDA-co-AM polymer films via X-ray diffraction.

Templating Effect of the Polymer Gel on Nucleation. The templating effect may affect crystal nucleation by aligning the solute molecules along the polymer chain via specific polymer−solute interactions. To capture specific polymer−solute interactions in a solvent environment realistically, we chose to determine the crystal facets preferentially grown from a polymer surface in the solvent of interest and infer the complementary functional group interactions by inspecting the molecular structures of surfaces in contact. Smooth and flat polymer films were prepared following the same formulation as used in the microgel synthesis, except that no porogen and solvent were added to the prepolymer mixture so as to minimize the variation in polymer mesh sizes, allowing us to focus on the polymer chemistry effect.

Shown in Figure 7a, PEGDA films preferentially templated the growth of the (002) plane of ASA and PEGDA-co-AM the (011) plane, judging from the relative peak intensities in the XRD patterns as compared with those of the bulk crystals. This result was corroborated by observations under an optical microscope that ASA crystals with elongated platelike shapes lay on their sides on the PEGDA surface via the (002) planes (Figure 7d,e) and stood tilted on the PEGDA-co-AM film via the (011) plane (Figure 7c). Comparing the molecular structures of (002) and (011) planes, it can be deduced that the methyl and phenyl groups of ASA (colored blue in Figure 7h) dominating the (002) plane interact mainly with the PEGDA polymer, and the carboxyl group (colored red in Figure 7h) characteristic of the (011) plane is responsible for interacting with the AM segments of PEGDA-co-AM. Such complementary interactions between PEGDA and ASA are possible because the phenyl and the methyl hydrogens of ASA, being next to electron-withdrawing groups, have increased tendency to interact with the oxygen of PEGDA. This type of C−H···O interaction, although much weaker than primary hydrogen bonding, is found to be abundant in many crystal systems,[26] such as the ASA crystal in which the methyl hydrogen interacts with the carbonyl oxygen in the ester group to form a dimerlike supermolecular synthon. However, one might expect that the carboxyl group instead of the phenyl and methyl groups of ASA should interact primarily with PEGDA via hydrogen bonding. This scenario is not observed, probably because the ASA carboxyl group is well solvated by ethanol and water, and as such, its interaction with PEGDA is hindered. As compared with PEGDA, the AM segments in the PEGDA-co-AM polymer carry a higher density of stronger hydrogen-bond acceptors in their amide moieties, which may be more effective in competing with ethanol and water to form hydrogen bonds with the ASA carboxyl groups. To summarize, the observed preferred crystal orientation induced by specific polymer−solute interactions provides strong evidence for the templating effect of the polymer film on nucleation. ASA interacts with PEGDA via weak C−H···O interactions, whereas its interaction with PEGDA-co-AM is much stronger, possibly via hydrogen

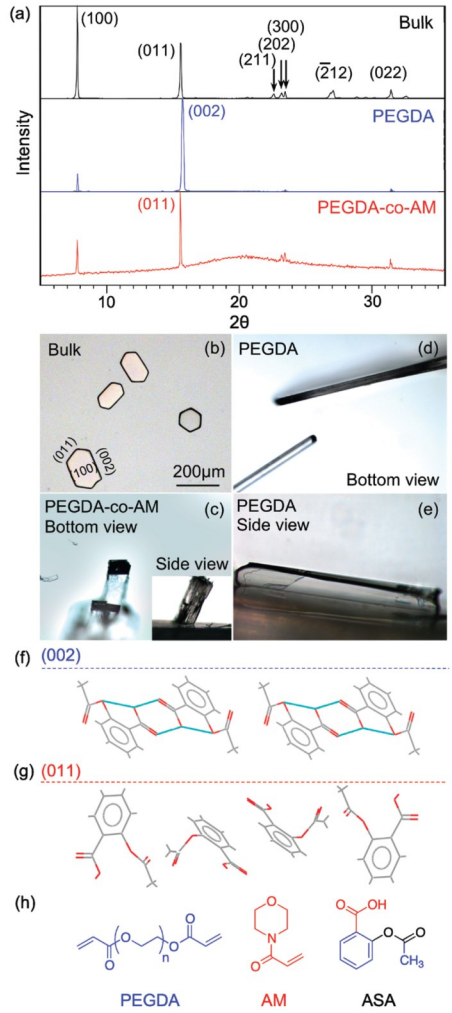

Figure 7. Preferred orientation of ASA crystals on polymer films. (a) Comparison of XRD patterns of ASA crystals grown from PEGDA and PEGDA-co-AM polymer films to that of bulk crystals obtained under the same crystallization conditions. The results are not sensitive to variations in *M*, and representative patterns are shown. The (002) peak is separated from the (011) peak by a 2θ angle of 0.17° (calculated from Cambridge Structure Database). The two peaks can be identified unambiguously given that the resolution of XRD measurement is 0.02°. (b–e) Optical images of ASA crystals nucleated from bulk (b), the PEGDA-co-AM surface (c), and the PEGDA surface (d and e). The scale bar is the same for all images. (f and g) Molecular structures of (002) and (011) facets of ASA crystal. The dotted line indicates the top surface of the corresponding facet. (h) Molecular structures of monomers of PEGDA, AM, and ASA. ASA functional groups colored blue are inferred to interact preferentially with PEGDA, and those colored red are inferred to interact with AM.

bonds formed between ASA and AM. This result is consistent with the observed higher ASA partitioning in PEGDA-co-AM and stronger binding between the two as measured by the ASA adsorption enthalpy on the polymer. Given the stronger interactions with one end of the ASA molecule than with the other, AM is likely to be more effective in aligning ASA molecules along the polymer chain and thereby lowers the entropic penalty for nucleus formation, leading to further shortened induction times.

Similarly, a preferred orientation of ACM crystals on polymer films was also observed, which further verifies the existence of a templating effect imposed by the polymer network. The XRD study showed that PEGDA induced growth of (011) and its higher index plane (022) almost exclusively, while PEGDA-co-AM preferentially templated $(10\bar{1})$ and its higher index plane $(20\bar{2})$ as well as $(11\bar{1})$ (Figure 8a). It is evident from the optical images (Figure 8b–e) that the prism-shaped ACM crystals exhibited random orientations when crystallized from bulk and seemed to assume certain through-plane orientations when nucleated on the respective films, judging from similar crystal morphology from the top view. Seen from the molecular structures of the templated crystal facets (Figure 8f–h), all planes present phenolic hydroxyl groups to the surface. On the other hand, the $(10\bar{1})$ and $(11\bar{1})$ planes are different in chemistry from (011) in that they better expose the amide group, although the difference is not as apparent as that between (002) and (011) of ASA. Such differences imply that after introducing AM into the PEGDA network, the polymer strengthens its interactions with ACM by forming hydrogen bonds with the amide group of ACM, in addition to those with the phenolic hydroxyl group. These observations can explain the moderate increase in partition coefficients after gel modification. Interestingly, both the amide and the phenolic hydroxyl groups with which AM preferentially interacts are also critical for forming the ACM crystal structure (form I), which is essentially a network of intermolecular hydrogen bonds between the two groups. This may suggest that with the ability to hydrogen bond with both of the groups in the solvent of interest, the AM segment could act like a "catalyst" for crystal nucleation by facilitating hydrogen bond formation between the aligned ACM molecules and lead to the fast nucleation process observed in the induction time study with modified gels (Table 2).

In conclusion, we have demonstrated the essential role of polymer–solute interactions in controlling solute nucleation by tuning the chemical composition of the polymer microgels used for inducing nucleation. When AM comonomer was introduced into the PEGDA matrix via copolymerization, ASA nucleation kinetics were promoted by up to 4 orders of magnitude, while nucleation of ACM was also enhanced by up to 2 orders of magnitude. The extent of nucleation acceleration generally correlates with the strength of the polymer–solute interactions as characterized by solute partition coefficients and adsorption enthalpies. Moreover, the effect of polymer–solute interactions on nucleation was manifested by the split of nucleation time scales due to the presence of nucleation sites of distinct chemical compositions in the microgels, inferred from SANS data. We further propose that favorable polymer–solute interactions promote nucleation by two means. First, it leads to a higher solute concentration in the gel, which enhances the effective solute–solute interactions. Second, specific polymer solute interactions, as evidenced by the preferred crystal orientation on polymers, facilitate molecular alignment along the polymer chain. Our results provide insights into the nucleation of molecular crystals at complex interfaces and help set the stage for rational design of "nucleants" to direct nucleation as desired.

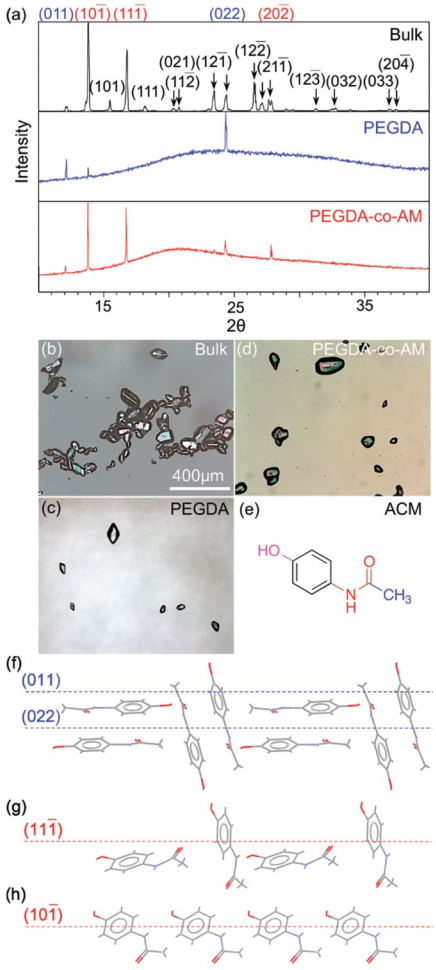

Figure 8. Preferred orientation of ACM crystals on polymer films. (a) Comparison of XRD patterns of ACM crystals grown from PEGDA and PEGDA-co-AM polymer films to that of bulk crystals obtained under the same crystallization conditions. All ACM crystals are form I, the monoclinic form. The miller indexes (*hkl*) of facets preferentially oriented parallel to the polymer surface are colored blue and red, corresponding to PEGDA and PEGDA-co-AM polymer films, respectively. (b–d) Optical images of ACM crystals nucleated from bulk (b), the PEGDA surface (c), and the PEGDA-co-AM surface (d). The scale bar is the same for all images. (e) ACM molecular structure. The functional group colored blue is inferred to interact preferentially with PEGDA, and those colored red are inferred to interact with AM. The group colored purple interacts with both PEGDA and AM. (f–h) Molecular structures of the (011), (022), (11$\bar{1}$), and (10$\bar{1}$) facets of the ACM crystal. Above the dotted line is the top surface of the corresponding facet.

EXPERIMENTAL SECTION

Materials. Poly(ethylene glycol) diacrylate with average molecular weights of M = 200, 400, 575, and 700 g/mol and tri(ethylene glycol) diacrylate (M = 130 g/mol), 4-acryloyl morpholine, poly(ethylene glycol) with M = 200 g/mol (PEG_{200}), 2-hydroxy-2-methyl-1-phenyl-propan-1-one (DC1173) photoinitiator, Tween20 nonionic surfactant, and ethanol (99.9%) were purchased from Sigma Aldrich Chemical Co. and used as received with no further purification. Deionized water (18.3 MΩ) was obtained using a Millipore Milli-Q purification system. For PEGDA microgel precursors, solutions containing 25% PEG_MDA, 25% PEG_{200}, and 5% DC1173 by volume in ethanol were prepared for each of the values of the molecular weight M used. Similarly, for PEGDA-co-AM microgels, solutions containing 15% PEG_MDA, 15% AM, 25% PEG_{200}, and 5% DC1173 photoinitiator by volume in ethanol were prepared for each of the values of the molecular weight M used. ASA (99%) was purchased from Alfa Aesar, and ACM (99.0%) was from Sigma Aldrich, both used without further purification. Perdeuterated ethanol (*d*-ethanol, 99.9%) was purchased from Cambridge Isotope Laboratories and used without further purification.

Microgel Synthesis. Cuboid microgel particles were synthesized by SFL.[27] Microfluidic channels with straight, rectangular cross-sections (width = 300 μm, height = 30 μm) were prepared by soft lithography. Briefly, polydimethylsiloxane (PDMS, Sylgard 184, Dow Corning) was poured on an SU-8 photoresist patterned silicon wafer and cured to create a bas-relief microchannel device. Channels with end reservoirs were cut from the wafer with a scalpel, and inlet and outlet ports were punched into the device with a blunt syringe (Small Parts, Inc.) to introduce the hydrogel precursors. A photomask featured with square shapes was designed using AUTOCAD and printed at 50800 dpi by FineLine Imaging (Colorado Springs, CO). For SFL, the microfluidic device was placed on a translating stage inverted microscope. The inlet channel was loaded with a hydrogel precursor using a pressure-controlled manifold. The mask was placed in the field-stop of the microscope, and square features were projected on the precursor by ultraviolet (UV) exposure from a Lumen 200 lamp (Prior) through a wide excitation UV filter set (11000v2: UV, Chroma) when the flow of precursor was stopped. The ultimate feature sizes of the patterned squares were 30 μm × 30 μm, determined through fluorescence imaging of the microchannel during UV illumination. Pulses of UV exposure were obtained by a computer-aided UV shutter (UniBlitz). Incident UV intensities were measured using a UVA Power and Dose meter (ACCU-CAL-30 UVA, DYMAX). In all experiments, the measured exposure was 0.89 μW, and the UV exposure time was fixed at 200 ms. Particles were collected through the outlet channel into a microcentrifuge tube reservoir containing 0.2% v/v Tween20 in a mixture of 62/38 water/ethanol (v/v). Tween20 was added to the outlet reservoir to render the microgels colloidally stable during purification.

SFL was performed until approximately 50000 particles were synthesized. The reservoir tube containing particles was then removed from the microfluidic device. The tube was placed in a minicentrifuge (Galaxy MiniStar, VWR Scientific) at 6000 rpm for 8 s to sediment the microgels. The supernatant was removed, and the particles were resuspended in 1 mL of a rinsing fluid and vortex mixed for 10 s. This procedure was repeated several times to eliminate any remaining unreacted prepolymer solution. The first three washes were performed using 62/38 water/ethanol (v/v) with 0.2% Tween20, and three final washes were performed using 62/38 water/ethanol (v/v) with no Tween20 to eliminate excess surfactant.

Equilibrium Swelling Measurements. Equilibrium swelling measurements were carried out using a procedure described previously.[9] Briefly, it was assumed that the as-synthesized dimensions of the microgels within the preparative microfluidic device were in the "relaxed" state (corresponding to a θ-solvent for the polymer), and their side length, L_0, was measured in situ. After purification and transfer into the appropriate crystallization solvent, the swollen side length, L, dimensions of the microgels were measured using DIC microscopy. These measurements were used to obtain the volumetric swelling ratio, $R = L/L_0$, assuming isotropic swelling of the microgel. Finally, the apparent average mesh size ξ was estimated using Flory–Rehner theory,[28] which gives the average PEG_MDA molecular weight between cross-links, $\bar{M}_c$, as

$$\frac{1}{\bar{M}_c} = \frac{2}{M} - \frac{\ln(1 - R\phi_{p,0}) + R\phi_{p,0} + \chi(R\phi_{p,0})^2}{\phi_{p,0}\rho_p V_s\left(R^{1/3} - \frac{R}{2}\right)} \quad (1)$$

where χ is the Flory χ parameter, ρ_p is the density of the polymer, and V_{-s} is the molar volume of the solvent. The quantity $\phi_{p,0}$ is the volume

dx.doi.org/10.1021/cg201434r | Cryst. Growth Des. 2012, 12, 508–517

fraction of polymer in the microgel, where we assume that the polymerization proceeds to completion, and thus, $\phi_{p,0}$ is equal to the volume fraction of monomers in the hydrogel precursor. Subsequently, the apparent, average mesh size of the hydrogel, ξ, is given by[28]

$$\xi = R\phi_{p,0}^{1/3}\left(\frac{2C\bar{M}_c}{\bar{M}_n}\right)^{1/2} l \quad (2)$$

where C is the characteristic ratio and l is the average bond length of the polymer. Estimations of ξ were carried out using model parameters for PEGDA in a water−ethanol (see the Supporting Information of ref 9). It was assumed that these model parameters were unchanged by either the PEGDA molecular weight or the presence of the comonomer AM. The latter is a particularly significant approximation and will be evaluated subsequently.

SANS. SANS was performed at the National Institute of Standards and Technology Center for Neutron Research (NCNR). Samples were prepared by loading hydrogel precursors (with the compositions previously described) for the $PEG_{200}DA$, $PEG_{700}DA$, $PEG_{200}DA$-co-AM, and $PEG_{700}DA$-co-AM microgels into standard titanium scattering cells with a path length of 1 mm. To polymerize the material, samples were irradiated with a hand-held UV lamp with an output intensity of 0.2 mW/cm^2 for 1 min, resulting in a total UV dose that is approximately equivalent to that supplied during SFL of microgel particles.

SANS measurements were carried out on the NG7 30 m SANS instrument with the 10CB sample environment. Temperature control was obtained using a Julaba temperature bath unit at 25 °C, and samples were left to equilibrate for at least 30 min prior to measurement. Scattering using incident neutrons of wavelength λ = 6 Å and a wavelength spread (fwhm) of $\Delta\lambda/\lambda$ = 11% was collected at detector distances of 1 m with 20 cm offset, 4 m, and 13.5 m for high q measurements. Scattering using incident neutrons of wavelength λ = 8.09 Å and a wavelength spread (fwhm) of $\Delta\lambda/\lambda$ = 11% was collected at a detector distances of 15.3 m for low q measurements. SANS measurements were performed on the BT5 perfect crystal diffractometer within the 6CB sample environment. Data were reduced using NIST IGOR software package[29] to obtain the absolute scattered intensity, $I(q)$. The incoherent background intensity, I_{bk}, was determined using a Porod analysis of the data at high q values.[29]

Partition Coefficient Measurements. Partition coefficients of ASA in PEGDA-co-AM gels from bulk solution were determined following a method similar to that described in our previous work.[9] In brief, a series of gels with varying mesh sizes of approximately 5 mm in diameter and 0.5 mm in thickness were synthesized via UV polymerization following the same formula as used in the microgel synthesis. The residue solvent, porogen, and monomer molecules were removed by extensive washing with solvent ethanol and subsequent vacuum drying. The dry gels were then immersed in an excess volume of 38 mg/mL ASA solution in 38/62 (v/v) ethanol/water at 15 °C for overnight. After equilibrium swelling was reached, the swollen gels were pad dried and dropped into an excess volume of water to release ASA. The total mass of ASA released was determined by measuring the equilibrium concentration of its degradation product in water, salicylic acid (SA), with UV−vis spectroscopy, after ASA aqueous solution was aged for a week to achieve complete hydrolysis. The ASA partition coefficient was calculated as the ratio of ASA mass fraction in solution absorbed by the gel to that in bulk solution. The partition coefficient of ACM was determined by the same method. The gels were immersed in 95 mg/mL ACM solution at 8 °C instead. Because ACM is stable in water, its concentration was determined directly after the swollen gel was immersed in water for 24 h. Three to four independent repeats were carried out for each type of sample to obtain the standard error of the partition coefficient.

Isothermal Titration Calorimetry (ITC). ITC measurements were performed on a TA Instruments NanoITC calorimeter. All experiments were performed at 23 °C using injections of ΔV = 10 μL of titrant, with a waiting time of 1000 s in between injections and 25 injections per measurement. For all measurements, the differential heat input, $q(t)$, was measured as a function of time t over all injections, followed by integration of $q(t)$ over each individual injection to obtain the molar heat of injection, $Q(T, P, c)$. The molar heat of injection can then be added cumulatively over all previous injections, yielding the total molar heat, Q_{tot} (T, P, c).

The primary measurement involves titration of a solution containing c_{inj} = 21 mg/mL ASA in 38/62 (v/v) ethanol/water (loaded in the injection syringe) into a suspension containing microgel particles at a concentration of 1 particle/μL in 38/62 (v/v) ethanol/water. For this process, the molar heat of injection contains several contributions

$$Q(T, P, c) = c_{inj}\Delta V[\Delta H_{ASA-gel}(T, P, c) + \Delta H_{dil}^{ASA}(T, P, c) + \Delta H_{dil}^{gel}(T, P, c)] \quad (3)$$

where $\Delta H_{ASA-gel}$ is the molar enthalpy of interaction between the ASA and the microgel particles, and ΔH_{dil}^{i} is the molar enthalpy of dilution of component i (ASA or gel, respectively) in 38/62 (v/v) ethanol/water. To determine $\Delta H_{ASA-gel}$, independent measurements of the ΔH_{dil}^{ASA} and ΔH_{dil}^{gel} were made by performing measurements where 21 mg/mL ASA in 38/62 (v/v) ethanol/water was injected into a sample containing only 38/62 (v/v) ethanol/water without particles and where 38/62 (v/v) ethanol/water without ASA was injected into a 1 particle/μL suspension 38/62 (v/v) ethanol/water. Subsequently, eq 3 was used to subtract the measured dilution enthalpies from the initial measurements of $Q(T, P, c)$ to obtain $\Delta H_{ASA-gel}$. Subsequently, the total, cumulative enthalpy evolved over all injections due to polymer−solute interactions, $\Delta H_{ASA-gel}^{tot}$, is calculated by summing the instantaneous enthalpy of interaction, $\Delta H_{ASA-gel}$, over all injections:

$$\Delta H_{ASA-gel}^{tot}(T, P, c) = \sum_{c_j=0}^{c} \Delta H_{ASA-gel}(T, P, c_j) \quad (4)$$

where c_j is the concentration of the j-th injection.

Nucleation Induction Time Measurement. Crystallization measurements of ASA from 38/62 (v/v) ethanol/water mixtures in the presence of PEGDA-co-AM microgels of various mesh sizes were conducted in an RS10 Clarity Solubility Station (Thermo Fisher Scientific). The detailed experimental procedure has been described elsewhere,[9] and the methodology is summarized as follows. Around 500 microgel particles were dispersed in every 1 mL of sample of a 38 mg/mL ASA solution in 38/62 (v/v) ethanol/water mixture and kept suspended by stirring the solution at 700 rpm. Ten such samples were loaded into the Clarity station at once and quench cooled to 15 °C to generate a supersaturation of 2.1. The onset of crystallization was signaled by the sudden drop in IR transmission signal through the solution. The time taken from the moment the desired supersaturation was achieved to the moment the IR signal dropped was taken to be the nucleation induction time. Ten samples were cycled 5−10 times to yield the induction time probability distribution. Experimental conditions were kept the same for samples with PEGDA gels and those with PEGDA-co-AM gels for direct comparison. During the experiments, the solution was inspected under the optical microscope at intervals to make sure the microgels were neither aggregated nor degraded. For ACM, the same procedures were followed with 95 mg/mL ACM solutions in 38/62 (v/v) ethanol/water cooled to 8 °C to achieve a supersaturation of 3.7.

Preferred Crystal Orientation via XRD. Polymer films of various PEG molecular weights were synthesized via UV polymerization using prepolymer mixtures of the same formulations as used for microgel synthesis but without adding solvent ethanol and porogen PEG200. Thirty microliters of prepolymer mixture was sandwiched between a glass slide and a quartz slide, both 75 mm × 25 mm in size. The glass slide was silanized with vinyl trichlorosilane, which copolymerizes with the monomer to graft the polymer film to the glass substrate via covalent bonds. The quartz slide was used as a template to make polymer films with the minimum surface roughness possible. The sandwiched prepolymer mixture was subjected to 70 mW/cm^2 UV light for 5 min to complete the polymerization, with the whole sample area irradiated fairly uniformly in the 5000-EC UV

Curing Flood Lamp (Dymax Corporation). The quartz slide was subsequently lifted to leave the flat and smooth polymer film conformed to the glass substrate. After synthesis, the polymer films were immersed vertically in 25 mg/mL ASA solution in 38/62 (v/v) ethanol/water mixture, which was filtered with a 0.45 μm PTFE membrane syringe filter before adding the polymer films. The solution was then sealed, cooled from 25 to 3 °C, and inspected visually every hour. Once crystals were spotted, the polymer film was withdrawn from the solution to terminate crystallization and immediately dipped into a DI water tank vertically to remove loosely attached crystals from the bulk solution (ASA is essentially insoluble in water at 3 °C). The back side of the glass substrate was used as a control to determine if all loose crystals were removed from the polymer film. Bulk crystals were obtained under the same conditions and served as the control sample for XRD analysis. For the ACM system, the same procedure was carried out with 80 mg/mL ACM solutions in 38/62 (v/v) ethanol/water mixture.

The specific crystal planes grown from the polymer film were analyzed using a PANalytical X'Pert PRO Theta/Theta Powder X-ray Diffraction System with Cu tube and X'Celerator high-speed detector. A sample area of 20 mm × 20 mm was irradiated with X-rays in one scan using a programmable divergence slit with 20 mm irradiated length and a 20 mm mask to ensure enough crystals on the polymer film were sampled to yield the statistically representative preferred orientation. Three scans were performed with one polymer film to cover almost the entire surface area. Because only the diffraction from the crystal plane parallel to the polymer film surface was seen by the X-ray detector, the peak that was significantly more intense relative to that of bulk crystals corresponded to the preferred nucleation face.

■ ASSOCIATED CONTENT

Supporting Information

Details of choice of polymer gel chemistry, polymer synthesis via SFL, and characterization of polymer gel microstructures via neutron scattering. This material is available free of charge via the Internet at http://pubs.acs.org.

■ AUTHOR INFORMATION

Corresponding Author

*E-mail: trout@mit.edu.

■ ACKNOWLEDGMENTS

We acknowledge the Novartis-MIT Continuous Manufacturing Center for financial support. We are indebted to Dr. Richard Sear from the University of Surrey for his insightful comments on quenched disorder phenomenon. His computational work inspired us to describe our experimental data using stretched exponentials. We are grateful to Prof. Karen Gleason for use of her equipment for glass silanization.

■ REFERENCES

(1) Debenedetti, P. G. *Metastable Liquids: Concepts and Principles*; Princeton University Press: Princeton, NJ, 1996.
(2) Hooks, D. E.; Fritz, T.; Ward, M. D. *Adv. Mater.* **2001**, *13*, 227.
(3) Berman, A.; Ahn, D. J.; Lio, A.; Salmeron, M.; Reichert, A.; Charych, D. *Science* **1995**, *269*, 515.
(4) Sommerdijk, N.; de With, G. *Chem. Rev.* **2008**, *108*, 4499.
(5) Aizenberg, J.; Black, A. J.; Whitesides, G. M. *Nature* **1999**, *398*, 495.
(6) Weissbuch, I.; Lahav, M.; Leiserowitz, L. *Cryst. Growth Des.* **2003**, *3*, 125.
(7) Gavish, M.; Wang, J. L.; Eisenstein, M.; Lahav, M.; Leiserowitz, L. *Science* **1992**, *256*, 815.
(8) Hiremath, R.; Basile, J. A.; Varney, S. W.; Swift, J. A. *J. Am. Chem. Soc.* **2005**, *127*, 18321.
(9) Diao, Y.; Helgeson, M. E.; Myerson, A. S.; Hatton, T. A.; Doyle, P. S.; Trout, B. L. *J. Am. Chem. Soc.* **2011**, *133*, 3756.
(10) Diao, Y.; Myerson, A. S.; Hatton, T. A.; Trout, B. L. *Langmuir* **2011**, *27*, 5324.
(11) Diao, Y.; Harada, T.; Myerson, A. S.; Hatton, T. A.; Trout, B. L. *Nat. Mater.* **2011**, *10*, 867.
(12) Jackson, C. L.; McKenna, G. B. *Chem. Mater.* **1996**, *8*, 2128.
(13) Ha, J. M.; Wolf, J. H.; Hillmyer, M. A.; Ward, M. D. *J. Am. Chem. Soc.* **2004**, *126*, 3382.
(14) Beiner, M.; Rengarajan, G. T.; Pankaj, S.; Enke, D.; Steinhart, M. *Nano Lett.* **2007**, *7*, 1381.
(15) Lang, M. D.; Grzesiak, A. L.; Matzger, A. J. *J. Am. Chem. Soc.* **2002**, *124*, 14834.
(16) Price, C. P.; Grzesiak, A. L.; Matzger, A. J. *J. Am. Chem. Soc.* **2005**, *127*, 5512.
(17) Cox, J. R.; Ferris, L. A.; Thalladi, V. R. *Angew. Chem., Int. Ed.* **2007**, *46*, 4333.
(18) Chayen, N. E.; Saridakis, E.; Sear, R. P. *Proc. Natl. Acad. Sci. U.S.A.* **2006**, *103*, 597.
(19) Nicholson, C. E.; Chen, C.; Mendis, B.; Cooper, S. J. *Cryst. Growth Des.* **2011**, *11*, 363.
(20) Helgeson, M. E.; Chapin, S. C.; Doyle, P. S. *Curr. Opin. Colloid Interface Sci.* **2011**, *16*, 106.
(21) Martin, J. E.; Wilcoxon, J.; Odinek, J. *Phys. Rev. A* **1991**, *43*, 858.
(22) Edholm, O.; Blomberg, C. *Chem. Phys.* **2000**, *252*, 221.
(23) Shibayama, M. *Macromol. Chem. Phys.* **1998**, *199*, 1.
(24) van Meel, J. A.; Sear, R. P.; Frenkel, D. *Phys. Rev. Lett.* **2010**, *105*, 4.
(25) Sear, R. P. *J. Phys.: Condens. Matter* **2002**, *14*, 3693.
(26) Steiner, T. *Chem. Commun.* **1997**, 727.
(27) Dendukuri, D.; Gu, S. S.; Pregibon, D. C.; Hatton, T. A.; Doyle, P. S. *Lab Chip* **2007**, *7*, 818.
(28) Peppas, N. A.; Hilt, J. Z.; Khademhosseini, A.; Langer, R. *Adv. Mater.* **2006**, *18*, 1345.
(29) Kline, S. R. *J. Appl. Crystallogr.* **2006**, *39*, 895.